Impedance Modeling and Stability Analysis of AC/AC Modular Multilevel Converter for Railway System

Wang, Yixing; Xu, Qianming; Liao, Shuhan; Wang, Lei; Guerrero, Josep M.

Published in:
IEEE Transactions on Transportation Electrification

DOI (link to publication from Publisher):
10.1109/TTE.2020.3043819

Publication date:
2021

Document Version
Accepted author manuscript, peer reviewed version

Impedance Modeling and Stability Analysis of AC/AC Modular Multilevel Converter for Railway System

Yixing Wang, Qianming Xu, *Member*, *IEEE*, Shuhan Liao, *Member*, *IEEE*,
Lei Wang, *Senior Member*, *IEEE*, Josep M. Guerrero, *Fellow*, *IEEE*

***Abstract*—The AC/AC MMC application in the electric railway poses new challenges to the stability of the railway system. The impedance analysis method is an effective way to assess the stability of AC/AC MMC-based railway systems. Due to the internal dynamics of AC/AC MMC, there are steady-state harmonic components in the arm currents and capacitor voltages, and these harmonic components have a significant impact on the dynamic characteristics and stability of AC/AC MMCs. To accurately predict the stability of AC/AC MMC-based railway systems, this paper proposes an impedance model of AC/AC MMC with consideration of dominate steady-state harmonics. Simulation and experimental results obtained from a prototype are presented to demonstrate the accuracy of the proposed impedance model. Besides, the proposed model is compared with the impedance model ignoring the steady-state harmonics, and the results show the advantage of the proposed model in the description of impedance characteristics of AC/AC MMCs. The stability of an example AC/AC MMC-based railway system is analyzed using the proposed model, and the stability analysis results are validated by simulations. The effect of control parameters on the impedance characteristics is further analyzed, and this provides the guidance for controller design to damp the instability of the system.**

***Index Terms*—Electric railway, AC/AC, modular multilevel converter (MMC), impedance model, stability**

I. Introduction

With the environmental constraints on the conventional transportation system, the electric railway system is considered to be one of the most eco-friendly and energy-efficient transportations [1]-[2]. In the last decade, the AC/AC MMC for railway power supply has drawn much attention due to its modularity, scalability, high efficiency, and superior harmonic performance [3]-[4]. In 2011, the first MMC-based railway traction power supply, consisting of two 37.5 MVA AC/AC MMC, was commissioned in Nuremberg, Germany [5]. Compared with the voltage source converter (VSC) for railway power supply, the AC/AC MMC can operate without the costly and bulky transformer and filter [6].

The interaction between the AC/AC MMC and the power electronic converter in the electric train may lead to oscillations across a wide frequency range, and thus poses new challenges to the railway system. To assess the harmonic stability of the AC/AC MMC-based railway system, the dynamic model of AC/AC MMC is essential to be established. Existing studies mainly focus on the steady-state model of AC/AC MMC for designing the controller of the MMC. A model of AC/AC MMC is proposed in [7]-[9]. The steady-state analysis [7] and the transient analysis [8]-[9] are conducted by this model to guide the design of control systems. However, the capacitor voltage dynamics are ignored in the model proposed in [7]-[9], which cannot reflect the internal dynamics of the MMC. References [10]-[11] establish a mathematical model of the AC/AC MMC considering the capacitor voltage dynamics, and the capacitor voltage-balancing control is designed based on this model to eliminate the imbalance of the arm-capacitor voltages. The above models [7]-[11] are adequate for the control design in ideal applications, e.g., AC/AC MMC connection with resistance-load, but cannot analyze the harmonic instability caused by the interaction between AC/AC MMC and power electronic converters in the electric railway application.

The impedance-based stability analysis is an effective method for the stability evaluation of the electric railway system [12]-[13], and the impedance model is the prerequisite for applying this stability analysis method. In recent years, most researchers have made efforts on the DC/AC MMC modeling [14]-[18]. Different from DC/AC MMCs, a single-phase side of AC/AC MMC is connected to AC network, instead of a dc link. Thus, the steady-state harmonic components in arm currents and capacitor voltages caused by internal dynamics are different in AC/AC MMCs and DC/AC MMCs, and the impedance modeling of DC/AC MMC cannot be directly extended to the impedance modeling on the AC/AC MMC. More recently, reference [19] presents an admittance model of AC/AC MMC. In [19], the admittance model of an AC/AC MMC is developed under a special case, where the steady-state capacitor voltage ripples have little effect on the admittance model. Thus, the steady-state capacitor voltage ripples are ignored in its admittance modeling. However, for other cases with different parameters, the dynamics of capacitor voltage ripples and current harmonic components can have significant impact on the stability of an AC/AC MMC system [20]. Therefore, it is significant to develop an impedance model of AC/AC MMC considering its steady-state harmonic components to accurately assess the stability of the AC/AC MMC-based railway system.

This paper develops an impedance model of AC/AC MMC

Manuscript received 23-May-2020; revised 10-Jul-2020 and 29-Sep-2020, 2020; accepted 02-Dec-2020. This work was supported by The National Natural Science Foundation of China under Grant 51807056. (Corresponding author: Qianming Xu)

Y. Wang, Q. Xu, S. Liao and L. Wang are with the College of Electrical and Information Engineering, Hunan University, Changsha 410082, China (e-mail: wang1809@hnu.edu.cn; hnuxqm@foxmail.com; shuhanliao@hnu.edu.cn; jordanwanglei@gmail.com).

J. M. Guerrero is with the Department of Energy Technology, Aalborg University, 9220 Aalborg East, Denmark (e-mail: joz@et.aau.dk).

Color versions of one or more of the figures in this paper are available online at http://ieeexplore.ieee.org.
Digital Object Identifier xx.xxxx/TTE.2020.xxxxxxx

with consideration of steady-state ripples of the capacitor voltages and arm currents harmonics. In Sections II, the steady-state model of AC/AC MMC is established. On this basis, the steady-state harmonics in the arm currents and capacitor voltages are obtained. Subsequently, Section III derives the impedance model of AC/AC MMC considering its steady-state internal harmonics based on the harmonic state-space (HSS) modeling method. Section IV verifies the developed impedance models by detailed circuit simulation and experimental measurements of a scaled-down prototype. Moreover, the proposed model is compared with the impedance model ignoring the steady-state harmonics, and the results show the advantage of the proposed model in the description of impedance characteristics of AC/AC MMC. In Section V, the stability analysis of the AC/AC MMC-based railway system is analyzed based on the proposed impedance model of single-phase side MMC. The effect of control parameters on the impedance characteristics is further analyzed, and the controller parameter design of MMC is guided to effectively improve the stability of the system. Section VI draws the conclusion.

II. Dynamic Model of AC/AC MMC

The configuration of a 50/3 Hz electric railway system with AC/AC MMC is shown in Fig. 1. Three-phase 110 kV 50 Hz grid voltages are stepped down to feed the AC/AC MMC through the traction transformer. The AC/AC MMC acts as the interface between the main grid and the traction network, converting the three-phase 50 Hz voltages to the single-phase 50/3 Hz railway voltage.

A. Averaged Model of AC/AC MMC

Fig. 2 illustrates the topology of AC/AC MMC, which converts the three-phase grid voltage $e(t)$ into the single-phase railway voltage $v_r(t)$ without a dc link. The converter consists of three-phase legs, and each phase-leg consists of one upper and one lower arm, where each arm comprises N submodules plus an arm inductance L_{arm} and a parasitic resistance R_{arm}. Each submodule (SM) consists of a capacitor C_{SM} and an IGBT full-bridge as a switching element. Note the full-bridge submodule is used to allow for inserting bipolar arm voltages, which is necessary for the direct AC/AC conversion.

Applying *Kirchhoff Voltage Law* to the circuit, the arm-current dynamics are described as

$$\begin{cases} e(t) - L_{arm}\dfrac{di_u(t)}{dt} - R_{arm}i_u(t) + v_u(t) = \dfrac{v_r(t)}{2} \\ e(t) + L_{arm}\dfrac{di_l(t)}{dt} + R_{arm}i_l(t) - v_l(t) = -\dfrac{v_r(t)}{2} \end{cases} \tag{1}$$

where $v_u(t)$ and $v_l(t)$ are the upper and lower arm voltage, $i_u(t)$ and $i_l(t)$ are the upper and lower arm currents. Due to a symmetrically similar relationship among three phases of AC/AC MMC, the subscript denoting the phase is dropped to simplify the notation.

The grid current $i_g(t)$ and the circulating current $i_c(t)$ are defined as

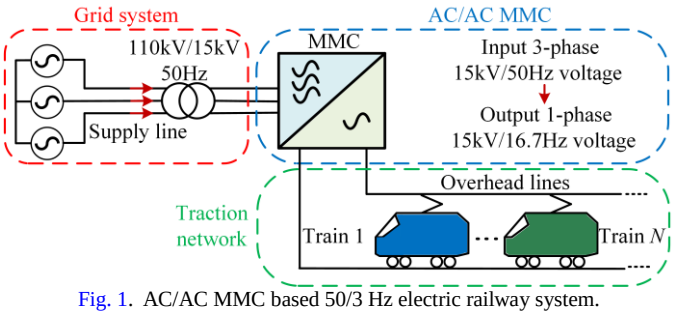

Fig. 1. AC/AC MMC based 50/3 Hz electric railway system.

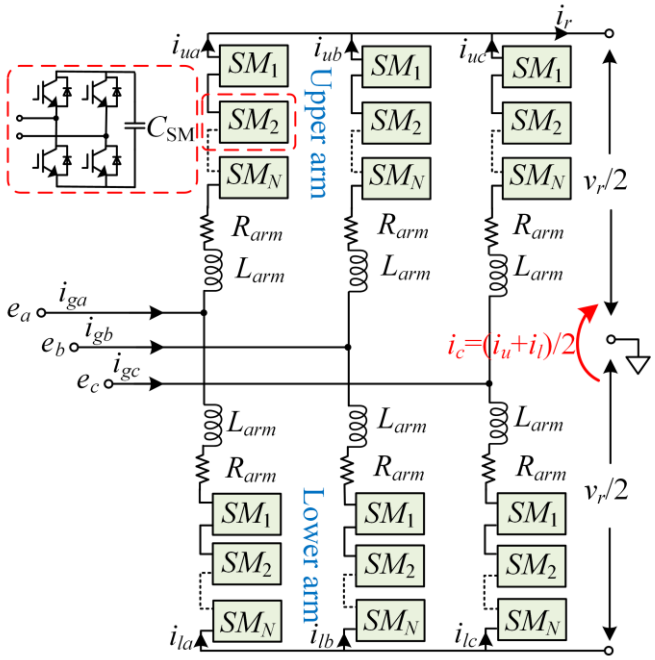

Fig. 2. AC/AC MMC topology with full-bridge submodules.

$$\begin{cases} i_g(t) = i_u(t) - i_l(t) \\ i_c(t) = \dfrac{i_u(t) + i_l(t)}{2} \end{cases}. \tag{2}$$

Combining (1) with (2), (1) can be rewritten as

$$\begin{cases} e(t) = \dfrac{L_{arm}}{2}\dfrac{di_g(t)}{dt} + \dfrac{R_{arm}}{2}i_g(t) + \dfrac{v_l(t) - v_u(t)}{2} \\ v_r(t) = -2L_{arm}\dfrac{di_c(t)}{dt} - 2R_{arm}i_c(t) + v_l(t) + v_u(t) \end{cases}. \tag{3}$$

Assuming the switching frequency is high enough and the SM capacitor voltages are always balanced, the MMC consisted of individual SMs can be treated as the averaged model [21]-[22]. Based on the averaged model, the arm voltages $v_{u,l}(t)$ and the sum of submodule capacitor voltages in the upper or lower arm $v_{Cu,l}^{\Sigma}(t)$ are obtained as

$$\begin{cases} v_{u,l}(t) = m_{u,l}(t)v_{Cu,l}^{\Sigma}(t) \\ C_{arm}\dfrac{dv_{Cu,l}^{\Sigma}(t)}{dt} = m_{u,l}(t)i_{u,l}(t) \end{cases} \tag{4}$$

where $C_{arm} = C_{SM}/N$, $m_{u,l}(t)$ are the modulation indices of upper and lower arms.

Combining (3)~(4), the state-space equation of AC/AC MMC can be obtained as

$$\dot{x}(t)=A(t)x(t)+B(t)u(t) \tag{5}$$

where

$$x(t)=\left[i_g(t),i_c(t),v_{Cu}^{\Sigma}(t),v_{Cl}^{\Sigma}(t)\right]^T \tag{6}$$

$$u(t)=\left[e(t),v_r(t)\right]^T \tag{7}$$

$$A(t)=\begin{bmatrix} -\frac{R_{arm}}{L_{arm}} & 0 & \frac{m_u(t)}{L_{arm}} & -\frac{m_l(t)}{L_{arm}} \\ 0 & -\frac{R_{arm}}{L_{arm}} & \frac{m_u(t)}{2L_{arm}} & \frac{m_l(t)}{2L_{arm}} \\ \frac{m_u(t)}{2C_{arm}} & \frac{m_u(t)}{C_{arm}} & 0 & 0 \\ -\frac{m_l(t)}{2C_{arm}} & \frac{m_l(t)}{C_{arm}} & 0 & 0 \end{bmatrix} \tag{8}$$

$$B(t)=\begin{bmatrix} 2/L_{arm} & 0 & 0 & 0 \\ 0 & -1/(2L_{arm}) & 0 & 0 \end{bmatrix}^T. \tag{9}$$

It can be observed from (4) that because of the multiplication between the arm current and modulation index, there are significant steady-state ripples in the capacitor voltage. The steady-state capacitor voltage ripples, which in turn create harmonic voltages across the arm inductor, lead to the harmonic components in the arm current. Clearly, this process resembles a "chain reaction" that causes an infinite number of steady-state harmonics in capacitor voltage and arm current, and the amplitude of harmonic becomes smaller as the frequency increases.

B. Harmonic steady-state study

In order to accurately represent the multi-harmonic characteristics of AC/AC MMCs at steady-state, the HSS modeling method [23]-[24], which is able to simultaneously represent multiple frequency responses, is introduced to model the AC/AC MMC. The modeling principle of the HSS method is provided in Appendix I.

Following the HSS modeling procedure, the time-domain model of the AC/AC MMC can be converted into the frequency-domain state-space equation:

$$s\boldsymbol{X}=(\boldsymbol{A}-\boldsymbol{N})\boldsymbol{X}+\boldsymbol{B}\boldsymbol{U} \tag{10}$$

where

$$\begin{aligned} \boldsymbol{X}&=\left[X_{-n},\cdots,X_{-1},X_0,X_1,\cdots,X_n\right]^T \\ X_{\pm n}&=\left[I_{g\pm n},I_{c\pm n},V_{Cu\pm n}^{\Sigma},V_{Cl\pm n}^{\Sigma}\right]^T \end{aligned} \tag{11}$$

$$\begin{aligned} \boldsymbol{U}&=\left[U_{-n},\cdots,U_{-1},U_0,U_1,\cdots,U_n\right]^T \\ U_{\pm n}&=\left[E_{\pm n},V_{r\pm n}\right]^T \end{aligned} \tag{12}$$

$$\boldsymbol{A}=\Gamma\left(A(t)\right) \tag{13}$$

$$\boldsymbol{B}=\Gamma\left(B(t)\right) \tag{14}$$

$$\boldsymbol{N}=diag\left[-jn\omega_1\boldsymbol{I},\cdots,-j\omega_1\boldsymbol{I},\boldsymbol{O},j\omega_1\boldsymbol{I},\cdots,jn\omega_1\boldsymbol{I}\right]. \tag{15}$$

where ω_1 is the fundamental angular frequency of the system. Note that the fundamental frequency of the AC/AC MMC system is set as 50/3 Hz, making it beneficial for the expansion of the harmonics in the frequency domain.

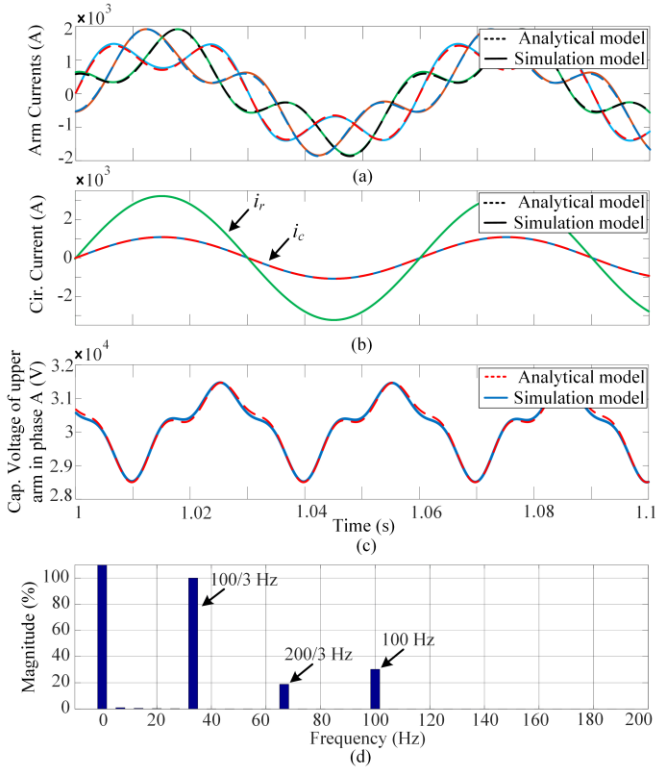

Fig. 3. Validation for the steady-state harmonic model of the AC/AC MMC. (a) Arm currents. (b) Circulating current. (c) Sum of submodule capacitor voltages of upper arm in phase A. (d) Frequency analysis of capacitor voltage.

TABLE I
PARAMETERS OF AN EXAMPLE AC/AC MMC

Symbol	Description	Value
e	Line to line RMS grid voltage	15 kV
v_r	Railway side voltage	15 kV
f_g	Grid frequency	50 Hz
f_1	Railway frequency	50/3 Hz
v_{C0}^{Σ}	Sum capacitor voltage	30 kV
N	Submodule number per arm	15
L_{arm}	Arm inductance	2 mH
R_{arm}	Arm parasitic resistance	0.5 Ω
C_{SM}	Submodule capacitance	15 mF

The harmonics of state variables at steady state can thus be calculated by setting the $s\boldsymbol{X}$ equaling to zero:

$$\boldsymbol{X}=-(\boldsymbol{A}-\boldsymbol{N})^{-1}\boldsymbol{B}\boldsymbol{U}. \tag{16}$$

To validate the steady-state harmonic model of AC/AC MMC, a comparison between the analytical model and the simulation in MATLAB/Simulink is shown in Fig. 3. The parameters of the MMC are listed in Table I. As can be seen, the analytical models match well with the simulation results, which verifies the steady-state model of the AC/AC MMC. The circulating current is equal to one-third of the single-phase side current, indicating the single-phase side current splits equally among three phases. The FFT analysis of the capacitor voltage in Fig. 3(d) shows there are mainly three steady-state ripples at $2f_1$, $f_g + f_1$ and $2f_g$ (e.g., 100/3 Hz, 200/3 Hz and 100 Hz) in the capacitor voltage. Based on the model, the steady-state harmonics of the AC/AC MMC for railway power supply can be accurately studied.

III. Impedance Modeling of AC/AC MMC

A. Harmonic Linearization

The impedance model of single-phase side AC/AC MMC is established by the harmonic linearization. A sinusoidal perturbation voltage v_{rp} at f_p is firstly injected in the single-phase voltage of AC/AC MMC. Then, the single-phase side impedance can be determined by calculating the corresponding single-phase side current response at the perturbation frequency.

By applying the harmonic linearization to the state-space equation of the AC/AC MMC in (5)-(9), the small-signal state-space equation of the MMC can be obtained as

$$\dot{x}_p(t) = A_p(t)x_p(t) + B_p(t)u_p(t) \tag{17}$$

where

$$x_p(t) = \left[i_{gp}(t), i_{cp}(t), v^{\Sigma}_{Cup}(t), v^{\Sigma}_{Clp}(t) \right]^T \tag{18}$$

$$u_p(t) = \left[m_{up}(t), m_{lp}(t), v_{rp}(t) \right]^T \tag{19}$$

$$A_p(t) = \begin{bmatrix} -\frac{R_{arm}}{L_{arm}} & 0 & \frac{m_{u0}(t)}{L_{arm}} & -\frac{m_{l0}(t)}{L_{arm}} \\ 0 & -\frac{R_{arm}}{L_{arm}} & \frac{m_{u0}(t)}{2L_{arm}} & \frac{m_{l0}(t)}{2L_{arm}} \\ \frac{m_{u0}(t)}{2C_{arm}} & \frac{m_{u0}(t)}{C_{arm}} & 0 & 0 \\ -\frac{m_{l0}(t)}{2C_{arm}} & \frac{m_{l0}(t)}{C_{arm}} & 0 & 0 \end{bmatrix} \tag{20}$$

$$B_p(t) = \begin{bmatrix} \frac{v^{\Sigma}_{Cu0}(t)}{L_{arm}} & -\frac{v^{\Sigma}_{Cl0}(t)}{L_{arm}} & 0 \\ \frac{v^{\Sigma}_{Cu0}(t)}{2L_{arm}} & \frac{v^{\Sigma}_{Cl0}(t)}{2L_{arm}} & -\frac{1}{2L_{arm}} \\ \frac{i_{g0}(t)/2 + i_{c0}(t)}{C_{arm}} & 0 & 0 \\ 0 & \frac{-i_{g0}(t)/2 + i_{c0}(t)}{C_{arm}} & 0 \end{bmatrix}. \tag{21}$$

in which the subscripts "0" and "p" denote the steady-state and perturbation components, respectively.

According to the internal dynamics of MMC, the injected perturbation voltage will result in the perturbations in all the state variables at ω_p, $\omega_p \pm \omega_1, \omega_p \pm 2\omega_1, \cdots, \omega_p \pm n\omega_1$. Applying the HSS modeling method, the small-signal model of the MMC in frequency domain can be obtained as

$$s\boldsymbol{X}_p = \left(\boldsymbol{A}_p - \boldsymbol{N}_p \right) \boldsymbol{X}_p + \boldsymbol{B}_p \boldsymbol{U}_p, \tag{22}$$

where

$$\begin{aligned} \boldsymbol{X}_p &= \left[X_{p-n}, \cdots, X_{p-1}, X_{p0}, X_{p1}, \cdots, X_{pn} \right]^T \\ X_{p\pm n} &= \left[I_{gp\pm n}, I_{cp\pm n}, V^{\Sigma}_{Cup\pm n}, V^{\Sigma}_{Clp\pm n} \right]^T \end{aligned} \tag{23}$$

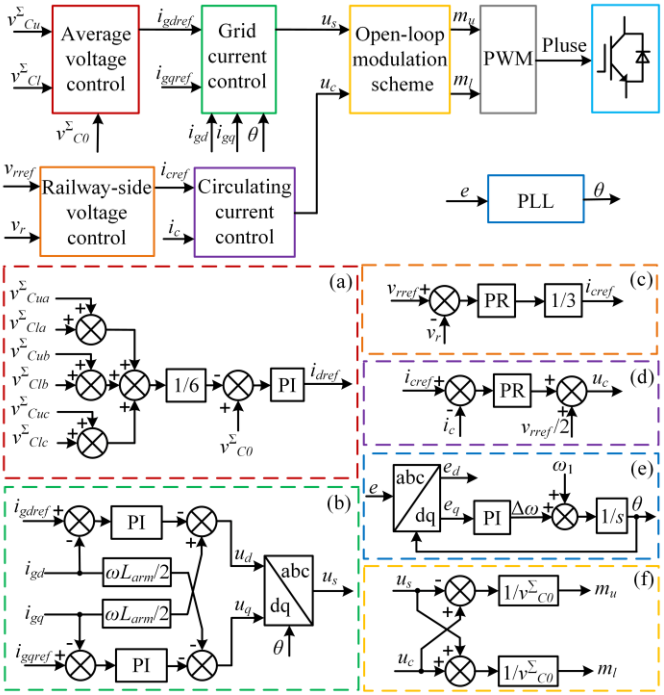

Fig. 4. Block diagram of the AC/AC MMC control scheme (a) Average voltage control. (b) Grid current control. (c) Railway-side voltage control. (d) Circulating current control. (e) PLL. (f) Open-loop modulation scheme.

$$\begin{aligned} \boldsymbol{U}_p &= \left[U_{p-n}, \cdots, U_{p-1}, U_{p0}, U_{p1}, \cdots, U_{pn} \right]^T \\ U_{p\pm n} &= \left[M_{up\pm n}, M_{lp\pm n}, V_{rp\pm n} \right]^T \end{aligned} \tag{24}$$

$$\boldsymbol{A}_p = \Gamma\left(A_p(t) \right), \boldsymbol{B}_p = \Gamma\left(B_p(t) \right) \tag{25}$$

$$\boldsymbol{N}_p = diag\left[j\left(\omega_p - n\omega_1 \right)\boldsymbol{I}, \cdots, \boldsymbol{O}, \cdots, j\left(\omega_p + n\omega_1 \right)\boldsymbol{I} \right]. \tag{26}$$

Note that the steady-state harmonics in the Toeplitz matrix $\boldsymbol{A}_p$ and $\boldsymbol{B}_p$ can be obtained by the steady-state harmonics model in Section II-B, or the simulation of the converter circuit. Furthermore, the perturbation modulation indices $M_{up\pm n}$ and $M_{lp\pm n}$ are related to the control dynamics of AC/AC MMC, which will be discussed in the following subsection.

B. Control Modeling

For the grid-side control of AC/AC MMC, due to the absence of a connection to a stiff dc bus, the capacitor voltage control is essential for the AC/AC MMC control scheme to maintain stable capacitor voltage. Fig. 4(a) shows the average voltage control to regulate the average of all SM capacitor voltages by using PI controller [10]. The PI controller produces the d-axis reference current. The q-axis reference current is set to be zero for unity power factor control. The grid current control in a rotating dq-frame is adopted to properly track the reference currents, as illustrated in Fig. 4(b). The phase-locked loop (PLL) strategy provides the controller with the estimated PCC voltage angle θ, and the structure of PLL is shown in Fig. 4(e).

For the railway-side control of AC/AC MMC, Fig. 4(c) shows the railway-side voltage control to provide a stiff voltage for the electric railway system by using a proportional resonant (PR) controller tuned at 50/3 Hz. As the zero-sequence current at 50/3 Hz inherently exists in the circulating current of the AC/AC MMC for railway power supply, a PR controller tuned

at 50/3 Hz is used to achieve zero steady-state errors for sinusoidal quantities, as shown in Fig. 4(d).

Furthermore, the open-loop modulation scheme, which can inherently stabilize the internal dynamics of MMC [25], is applied in this paper. Based on the modulation scheme, the modulation indices of upper and lower arms are expressed as

$$\begin{cases} m_u(t)=\left[-u_s(t)+u_c(t)\right]/v_{C0}^{\Sigma} \\ m_l(t)=\left[u_s(t)+u_c(t)\right]/v_{C0}^{\Sigma} \end{cases}, \tag{27}$$

where v_{C0}^{Σ} is the reference sum capacitor voltage with a constant value, $u_s(t)$ and $u_c(t)$ are the voltages from the grid-side control and railway-side control, respectively.

The control scheme of AC/AC MMC is mainly composed of the average voltage control, grid current control, PLL, railway-side voltage control, and circulating current control. Note that the grid-side of AC/AC MMC is treated as the strong grid in this paper. The grid voltage is hardly influenced by the perturbation voltage in the single-phase side, and the response of the detected phase θ in PLL is hardly influenced by the single-phase side perturbation voltage. Therefore, the PLL dynamics can be ignored in the impedance modeling of single-phase side AC/AC MMC. Based on the discussion above, the control model of AC/AC MMC is equal to the superposition of four control loops, and the small-signal control model is expressed as

$$\begin{cases} \boldsymbol{m}_{up} = -\boldsymbol{H}_g\boldsymbol{i}_{gp} - \boldsymbol{H}_c\boldsymbol{i}_{cp} - \boldsymbol{H}_r\boldsymbol{v}_{rp} - \boldsymbol{T}\left(\boldsymbol{v}_{Cup}^{\Sigma} + \boldsymbol{v}_{Clp}^{\Sigma}\right) \\ \boldsymbol{m}_{lp} = \boldsymbol{H}_g\boldsymbol{i}_{gp} - \boldsymbol{H}_c\boldsymbol{i}_{cp} - \boldsymbol{H}_r\boldsymbol{v}_{rp} + \boldsymbol{T}\left(\boldsymbol{v}_{Cup}^{\Sigma} + \boldsymbol{v}_{Clp}^{\Sigma}\right) \end{cases}, \tag{28}$$

where

$$\boldsymbol{m}_{up} = \left[M_{up-n},\cdots,M_{up-1},M_{up0},M_{up1},\cdots,M_{upn}\right]^T. \tag{29}$$

$\boldsymbol{m}_{lp}$, $\boldsymbol{v}_{rp}$, $\boldsymbol{i}_{gp}$, $\boldsymbol{i}_{cp}$, $\boldsymbol{v}_{Cup}^{\Sigma}$ and $\boldsymbol{v}_{Clp}^{\Sigma}$ follow the similar expressions as $\boldsymbol{m}_{up}$. $\boldsymbol{H}_g$, $\boldsymbol{H}_c$, $\boldsymbol{H}_r$, and $\boldsymbol{T}$ are the coefficient matrixes of the grid current control, the circulating current control, the railway-side voltage control, and the average voltage control, respectively.

1) Circulating Current Control

The circulating current control response to the small-signal modulation indices can be modeled by

$$\boldsymbol{m}_{up} = -\boldsymbol{H}_c\boldsymbol{i}_{cp}; \boldsymbol{m}_{lp} = -\boldsymbol{H}_c\boldsymbol{i}_{cp}, \tag{30}$$

where $\boldsymbol{H}_c$ is a $(2n+1)\times(2n+1)$ diagonal matrix expressed as

$$\begin{aligned} \boldsymbol{H}_c &= diag\left[\left\{q_k\right\}\big|_{k=-n,\cdots,0,\cdots,n}\right] \\ q_k &= H_c\left(j\left(\omega_p + k\omega_1\right)\right). \end{aligned} \tag{31}$$

H_c is the transfer function of the PR controller in the circulating current control.

2) Railway-side Voltage Control

The model of the railway-side voltage control is expressed as

$$\boldsymbol{m}_{up} = -\boldsymbol{H}_r\boldsymbol{v}_{rp}; \boldsymbol{m}_{lp} = -\boldsymbol{H}_r\boldsymbol{v}_{rp}, \tag{32}$$

where $\boldsymbol{H}_r$ is a $(2n+1)\times(2n+1)$ diagonal matrix expressed as

$$\boldsymbol{H}_r = diag\left[0,\cdots,0,H_{rv}\left(j\omega_p\right)H_c\left(j\omega_p\right),0,\cdots,0\right]. \tag{33}$$

H_{rv} is the transfer function of PR controller in railway-side voltage control.

3) Grid Current Control

Since the zero-sequence components will not flow among the three-phase three-line grid system, the grid current control only reacts to the positive and negative components. The sequence of small-signal components under single-phase voltage perturbation has following two features: (1) The single-phase side voltage is seen as the zero-sequence voltage with respect to the three-phase grid voltage; (2) The perturbation voltage added on the single-phase side has the same effect on the six arms and does not affect sequence relationship. Therefore, the sequence relationship of small-signal components is only determined by the sequence relationship of the grid voltage. Then $m\omega_g$ is introduced to the angular frequency of the perturbation current for analyzing the sequence relationships of the perturbation currents. The frequency of the perturbation current, which is $\omega_p \pm n\omega_1$, can be rewritten by using the modulo-2 function as mod(m,2)

$$\omega_p + \left(m\omega_g \pm \left|\mathrm{mod}\left(m,2\right)\right|\omega_1\right). \tag{34}$$

The sequence of the perturbation currents can be defined by using the modulo-3 function as mod(m, 3), given as

$$\mathrm{mod}\left(m,3\right) = \begin{cases} +1, m = 3i+1 \\ -1, m = 3i-1 \\ 0, m = 3i \end{cases} \tag{35}$$

where +1 indicates the positive sequence, −1 indicates the negative sequence, and 0 indicates the zero sequence. Based on the sequence relationships of harmonics, the model of the grid current control can be expressed as

$$\boldsymbol{m}_{up} = -\boldsymbol{H}_g\boldsymbol{i}_{gp}; \boldsymbol{m}_{lp} = \boldsymbol{H}_g\boldsymbol{i}_{gp}, \tag{36}$$

where

$$\begin{aligned} \boldsymbol{H}_g &= diag\left[\left\{q_m\right\}\big|_{m=-i,\cdots,0,\cdots,i}\right] \\ q_m &= \left|\mathrm{mod}\left(m,3\right)\right|\cdot\left[-\mathrm{mod}\left(m,3\right)jK_d + \right. \\ &\left. H_i\left(j\left[\omega_p + \left(m\omega_g \pm \left|\mathrm{mod}\left(m,2\right)\right|\omega_1\right)\right] - j\,\mathrm{mod}\left(m,3\right)\omega_g\right)\right]. \end{aligned} \tag{37}$$

H_i is the transfer function of the PI controller in current control, the jK_d term indicates the effects of the decoupling gain. The term $|\mathrm{mod}(m,3)|$ is used to remove the zero-sequence harmonics.

4) Average Voltage Control

As the sum of the capacitor voltages among three phases cancels the positive- and negative-sequence components in the capacitor voltage, only the zero-sequence perturbation voltages need to be concerned in the average voltage control. Then the model of average voltage control can be expressed as

$$\boldsymbol{m}_{up} = -\boldsymbol{T}\left(\boldsymbol{v}_{Cup}^{\Sigma} + \boldsymbol{v}_{Clp}^{\Sigma}\right); \boldsymbol{m}_{lp} = \boldsymbol{T}\left(\boldsymbol{v}_{Cup}^{\Sigma} + \boldsymbol{v}_{Clp}^{\Sigma}\right) \tag{38}$$

where

$$\begin{aligned} \boldsymbol{T} &= diag\left[\left\{q_m\right\}\big|_{m=-i,\cdots,0,\cdots,i}\right] \\ q_m &= \frac{1+(-1)^{|\mathrm{mod}(m,3)|}}{2}\cdot\left[H_v\left(j\left[\omega_p + \left(m\omega_g \pm \left|\mathrm{mod}\left(m,2\right)\right|\omega_1\right)\right]\right)\times\right. \\ &\left. H_i\left(j\left[\omega_p + \left(m\omega_g \pm \left|\mathrm{mod}\left(m,2\right)\right|\omega_1\right)\right]\right)\right] \end{aligned} \tag{39}$$

H_v is the transfer function of the PI controller in average voltage control. Note that q_m is zero for |mod(m,3)| = ±1, because average voltage control does not react to the positive- and negative-sequence components in the capacitor voltage.

C. Impedance Modeling of AC/AC MMC

Substituting the control model into the small-signal model of AC/AC MMC in (22), the perturbation state variables can be solved as

$$\boldsymbol{X}_p = \left(\boldsymbol{A}_p - \boldsymbol{N}_p\right)^{-1} \boldsymbol{B}_p \boldsymbol{U}_p \tag{40}$$

It is noted that the higher order of harmonics considered in the small-signal model, the higher accuracy can be achieved. However, the high harmonic order increases the complexity of the system model. As shown in Fig. 3, the steady-state harmonics above 100 Hz are quite small and can be nearly neglected. Thus, the harmonic order considered in the small-signal model of AC/AC MMC is set as n = 7.

The small-signal impedance of railway-side AC/AC MMC is obtained by calculating the ratio of the complex voltage to the resulting current at the perturbation frequency, which is defined as

$$Z_{\mathrm{MMC}}(s) = V_{rp}\left(f_p\right) \big/ I_{rp}\left(f_p\right) \tag{41}$$

As the single-phase current is three times the value of the circulating current, the impedance of the AC/AC MMC can be rewritten as

$$Z_{\mathrm{MMC}}(s) = V_{rp0} \big/ \left(3I_{cp0}\right), \tag{42}$$

The perturbation circulating current at f_p, which is depicted as I_{cp0}, is extracted from the perturbation components solved by (40).

IV. Simulation and Experimental Verifications

A. Simulation Validation

The accuracy of the developed model is first validated by the simulation. In the simulation, a nonlinear time-domain simulation model of AC/AC MMC is built in MATLAB/Simulink. The three-phase terminals of the MMC are connected to ideal voltage sources, and the single-phase terminal is connected to the resistive load. The single-phase side impedance of the AC/AC MMC is measured by injecting a series of small-signal perturbation voltages at different frequencies in the single-phase voltage. Then the AC/AC MMC impedance can be obtained by calculating the ratio of the perturbation voltage to the corresponding current at each frequency. The main parameters of the AC/AC MMC in the simulation are the same as Table I. The control parameters in the simulation are listed in Table II.

Fig. 5 shows the comparison of the simulation and analytical results of AC/AC MMC single-phase side impedance. The red curve corresponds to the proposed impedance model, and the responses obtained from circuit simulation are presented by circles at discrete frequency points. It can be observed the simulation measurements exhibit good overall matching to the analytical impedance model, indicating the accuracy of the proposed impedance.

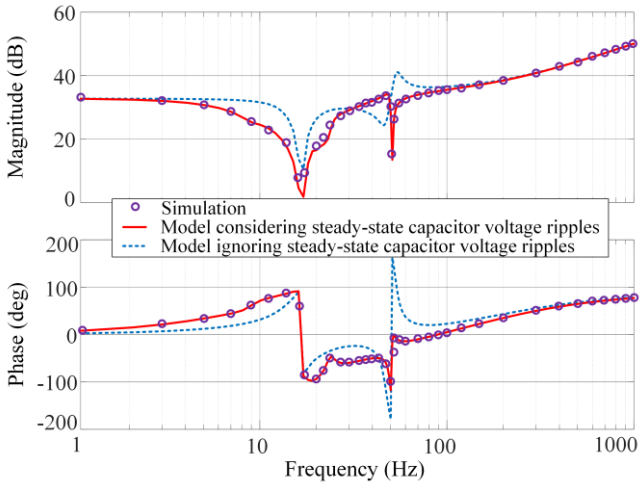

Fig. 5. Impact of the steady-state capacitor voltage ripples in the modeling on the accuracy of the analytical impedance model.

TABLE II
Control Parameters of AC/AC MMC

Symbol	Description	Value
$H_i(s)$	Grid current controller	1+10/s
$H_c(s)$	Circulating current controller	$1+10s/(s^2+\omega_1^2)$
$H_{rv}(s)$	Railway-side voltage controller	$0.5+s/(s^2+\omega_1^2)$
$H_v(s)$	Average voltage controller	0.5+10/s

Moreover, the impact of the steady-state capacitor voltage ripples in the modeling on the accuracy of the analytical AC/AC MMC impedance model is also shown in Fig. 5. The blue dashed curve corresponds to the impedance model ignoring the steady-state capacitor voltage ripples. It can be observed that when the steady-state capacitor voltage ripples are ignored in the impedance modeling of AC/AC MMC, the model is significantly different from the actual responses, especially below 100Hz. Therefore, it is essential to consider the steady-state capacitor voltage ripples in the impedance modeling in order to accurately reveal the characteristics of AC/AC MMC impedance model.

B. Experimental Validation

To further validate the steady-state harmonic analysis and the impedance model of AC/AC MMC, a 10kVA down-scaled AC/AC MMC is developed in the laboratory. The topology of the MMC experimental setup is shown in Fig. 6. The digital control system is implemented by DSP (TMS320F2812) and FPGA (EP2C8), which integrates a programmable logic with a processing system. The parameters of the down-scaled prototype are given in Table III.

In order to obtain the waveforms of AC/AC MMC under the steady-state operation condition, the MMC is firstly operated in the steady state, where the single-phase terminal is connected to the resistive load. Fig. 7 shows the experimental waveforms. It is obvious in Fig. 7 that the arm currents contain the components of the grid current at 50 Hz and the single-phase side current at 50/3 Hz, and the submodule capacitor voltages contain the obvious steady-state ripples.

To validate the proposed impedance model of single-phase side AC/AC MMC, the small-signal impedance measurements are carried out on a down-scaled AC/AC MMC experimental setup. The resistor load is connected to the single-phase side of

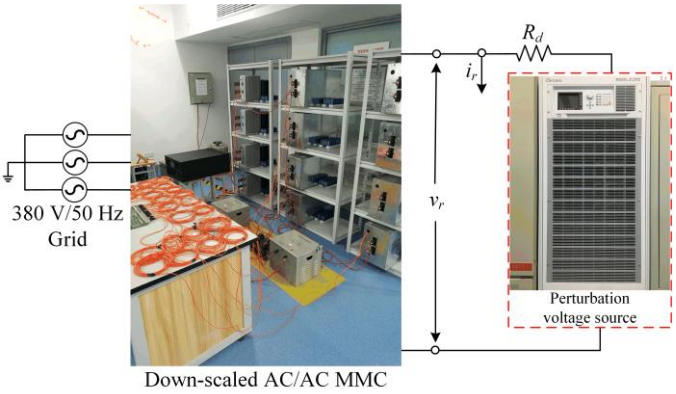

Fig. 6. Schematic diagram of the experimental setup.

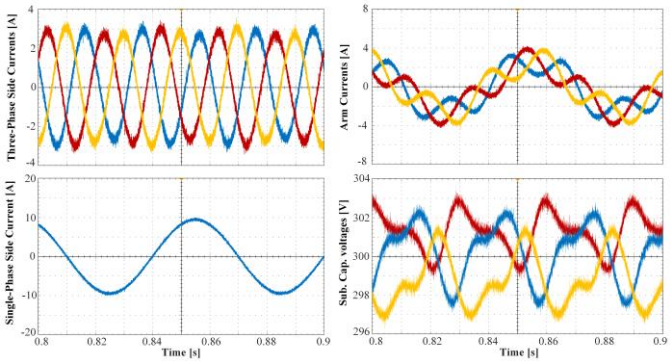

Fig. 7. Experimental results of the AC/AC MMC under steady-state operation condition.

TABLE III
PARAMETERS OF SCALE-DOWN PROTOTYPE

Power supply parameters		
e	Line to line RMS grid voltage	1 p.u. (380 V)
f_g	Three-phase frequency	50 Hz
f_1	Single-phase frequency	16.7 Hz
v_{C0}^{Σ}	Sum capacitor voltage	1.6 p.u.
N	Submodule number	2
L_{arm}	Arm inductance	0.04 p.u.
C_{SM}	Submodule capacitance	0.04 p.u.
R_L	Load resistance	0.7 p.u.
Controller parameters		
$H_i(s)$	Grid current controller	$0.1+1/s$
$H_c(s)$	Circulating current controller	$0.1+0.5s/(s^2+\omega_1^2)$
$H_{rv}(s)$	Single-phase side voltage controller	$0.05+0.1s/(s^2+\omega_1^2)$
$H_v(s)$	Average voltage controller	$0.5+1/s$

the AC/AC MMC to determine the steady-state operating point. The Chroma 61611 programmable AC source is used as the voltage source to inject the perturbation voltage to the single-phase side voltage at 50/3 Hz. The programmable AC source performs the frequency sweeps ranging from 1 Hz to 1000 Hz superposed on the 50/3 Hz fundamental frequency. Then, the resulting perturbation voltage and current are extracted. The impedance of single-phase side AC/AC MMC is calculated by the ratio of the perturbation voltage to current as

$$Z_{\mathrm{MMC}}\left(f_p\right)=V_r\left(f_p\right)/I_r\left(f_p\right) \tag{43}$$

where $V_r(f_p)$ and $I_r(f_p)$ are the Fourier components of single-phase side voltage v_r and current i_r, respectively, at frequency f_p.

The proposed analytical impedance model of AC/AC MMC is compared with the experimental measurement impedance, as shown in Fig. 8. The blue curve corresponds to the analytical impedance model of single-phase side AC/AC MMC. The responses obtained from experimental measurements are presented by red circles at discrete frequency points. It can be seen from Fig. 8, the experimental measurements are well matching the analytical impedance model, which confirm the validity of the proposed impedance models.

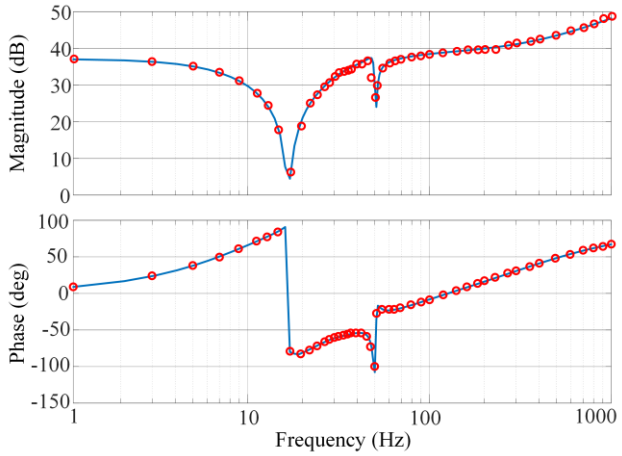

Fig. 8. Validation of the impedance responses of the AC/AC MMC by comparing the developed impedance model (blue solid line) to the experimental measurements (red circles).

V. STABILITY ANALYSIS OF AC/AC MMC-BASED RAILWAY SYSTEM

A. Stability analysis

Based on the presented impedance model, the stability of the AC/AC MMC-based railway system can be analyzed via the impedance-based stability criterion. Fig. 9 shows the structure diagram of AC/AC MMC based railway system connected to electric trains. The catenary is generally adopted in the traction network, which is equivalent to the resistance–inductance circuit model. The traction drive system of electric train consists of the onboard transformer, single-phase 4-quadrant converters (4QC), dc-link capacitors, three-phase inverters, and induction motors [26]. When the stability issue at the traction network is considered, the inverters and induction motor are equivalent to a load resistance [27]. Besides, the impedance model of single-phase VSC in the stationary frame has been fully investigated in [28]-[29], so it is not presented.

The small-signal impedance model of the interconnected system is shown in Fig. 10. As shown in Fig. 10, the ideal voltage source $V_s(s)$ in series with the MMC impedance $Z_{\mathrm{MMC}}(s)$ represents the AC/AC MMC; $Z_c(s)$ is the impedance of the catenary network between the MMC and the electric trains; the current source $I_t(s)$ in parallel with the impedance $Z_t(s)$ represents the electric train. In order to investigate the interaction behaviors of the traction network in the same voltage level, the train impedance at the secondary side should be converted to the primary-side of the traction network, i.e., $Z_T(s) = k^2\, Z_t(s)$ where k is the onboard transformer ratio. For simplicity, the electric trains are aggregated into one train, and the equivalent train-side impedance is obtained as $Z_{eq}(s) = Z_T(s)/N$, where N is the number of the trains. Then, the voltage at the interconnection point is given by

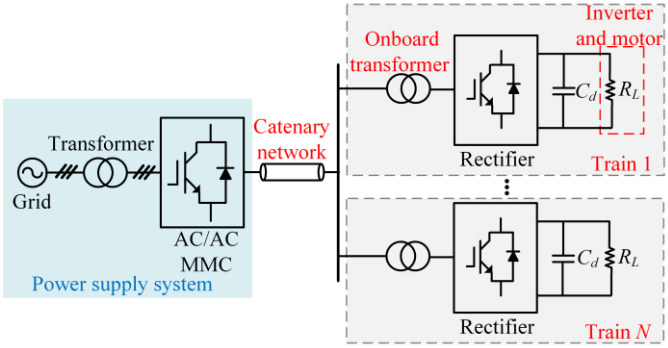

Fig. 9. Structure diagram of AC/AC MMC based railway system.

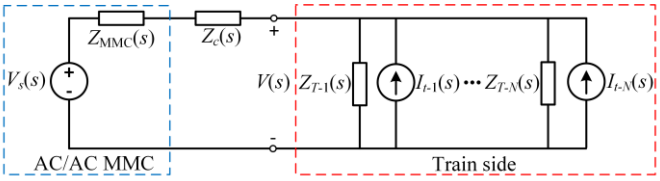

Fig. 10. Small-signal impedance model of the AC/AC MMC based railway system.

$$V(s)=\left[\left(Z_{\mathrm{MMC}}(s)+Z_c(s)\right)NI_t(s)+V_s(s)\right]\times \left[\frac{1}{1+\left(Z_{\mathrm{MMC}}(s)+Z_c(s)\right)/Z_{eq}(s)}\right] \quad (44)$$

In order to determine the system stability, it is assumed that: 1) $V_s(s)$ is stable in the open-circuit conditions, and 2) $I_t(s)$ is designed to be stable when the voltage source impedance is zero. Then the system small-signal stability is determined by the impedance ratio $(Z_{\mathrm{MMC}}(s)+Z_c(s))/Z_{eq}(s)$. This impedance ratio should satisfy the Nyquist stability criterion if the system is stable [12].

Fig. 11 shows the impedance-frequency characteristics of the single-phase side AC/AC MMC and the equivalent train-side impedance under different trains (e.g., $N = 2$, $N = 4$, $N = 6$ and $N = 10$). The parameters of the electric train system are listed in Table IV in Appendix II. Applying the Nyquist criterion, the stability of the AC/AC-MMC-based railway system can be assessed. It can be seen from Fig. 11, the phase margin of the system becomes smaller with the increasing number of trains in operation. When the number of trains is 2, the stability margin of the system is about 60 °, meaning the system is stable. When the operating trains are 10, the MMC impedance intersects the train-side impedance at 50 Hz with the stability margin less than zero, indicating the system is unstable and the oscillations will arise at 50 Hz.

Due to the complexity of the practical system, the simulation is considered to be an acceptable method to verify the stability analysis of the system. Fig. 12 shows the simulation results of the MMC-based railway system under 2 operating trains. It can be seen that the system is stable without the harmonic voltage and current. Fig. 13 shows the simulation results of the railway system under 10 operating trains. It is obvious that there are oscillations in the overhead line voltage and current. Furthermore, the FFT result of the overhead line voltage shows that the dominant oscillation frequency is 50 Hz, which confirms the instability analysis based on the impedance model.

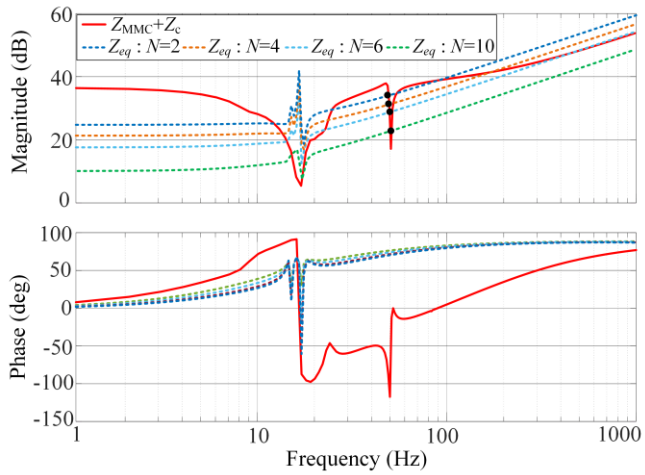

Fig. 11. Impedance characteristics of the AC/AC MMC and the train-side impedance under different trains.

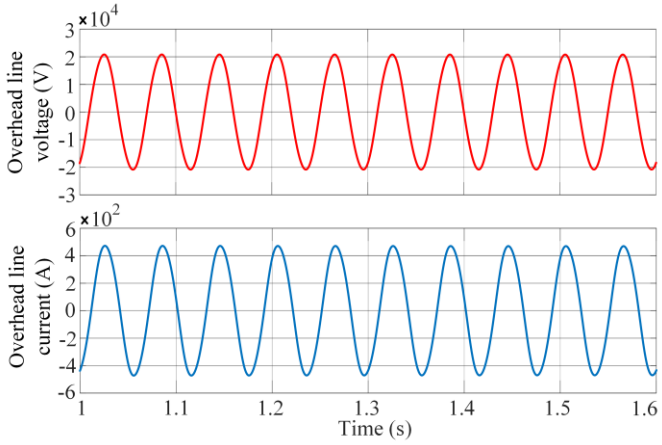

Fig. 12. Simulation results of overhead line voltage and current under 2 operating trains.

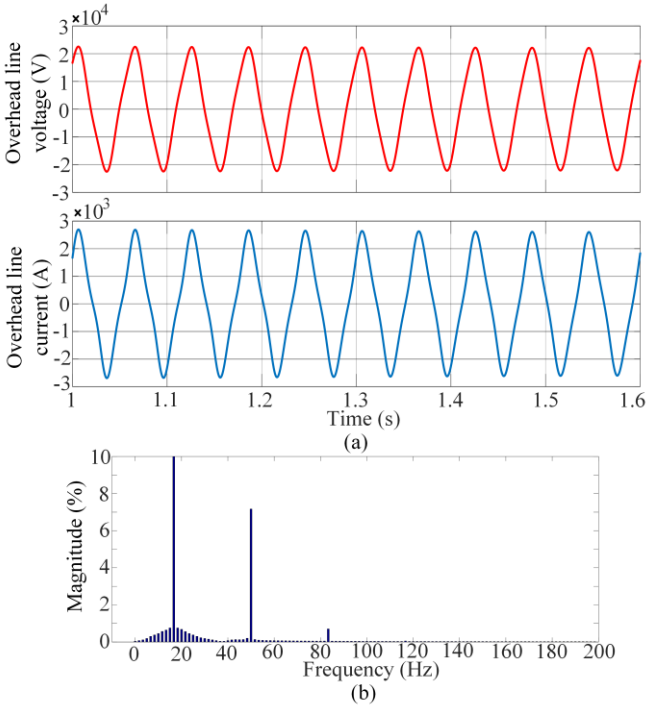

Fig. 13. Simulation results of overhead line voltage and current under 10 operating trains.

Fig. 14 shows the impact of the steady-state capacitor voltage ripples in the modeling of AC/AC MMC on the stability analysis of the MMC-based railway system. It can be observed that the red curve (impedance model considering the steady-state capacitor voltage ripples) intersects the train system impedance at 50 Hz with the phase margin less than zero, which indicates the system is unstable. However, if the steady-state capacitor voltage ripples are ignored in the modeling, the impedance model of MMC corresponding to the blue dashed curve does not intersect the train system impedance, which indicates the system should be stable. Yet, the simulation results as shown in Fig. 13 indicate that the system is actually unstable. Therefore, the steady-state capacitor voltage ripples should be considered in the impedance modeling of single-phase side AC/AC MMC to assess the stability of the system accurately.

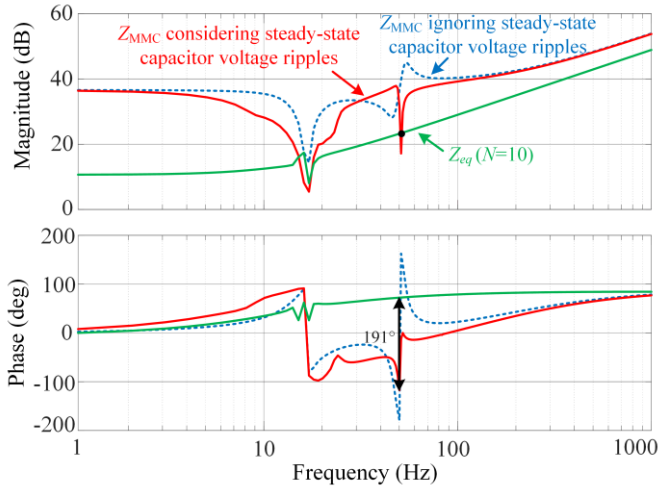

Fig. 14. Comparison of stability analysis with and without considering the steady-state capacitor voltage ripples in the impedance modeling of AC/AC MMC.

B. Design guidance of the AC/AC MMC controller

In the AC/AC MMC-based railway system, the stability of the system can be guaranteed by adjusting the control parameters of the AC/AC MMC and the converter in the electric trains. Considering the practical application, modifying the controller parameters of the electric trains will be applied in a number of trains. Thus, adjusting the controller parameters of MMC is easy to carry out in practice. Fig. 15 shows the effect of the proportional gain of the railway-side voltage controller on the single-phase side impedance of the MMC. It can be observed that decreasing proportional gain leads to the smaller magnitude of the MMC impedance, except for the two resonance points at 50/3 Hz and 50 Hz. Moreover, the phase of the AC/AC MMC impedance around 50 Hz is greatly increased with the decreasing proportional gain, thereby increasing the stability margin of the system. It can be seen from Fig. 15, when the proportional gain decreases from 1 to 0.25, the phase margin of the system increases from less than 0 °to greater than 20 °. Thus, the system stability can be effectively improved by decreasing the proportional gain of the railway-side voltage controller.

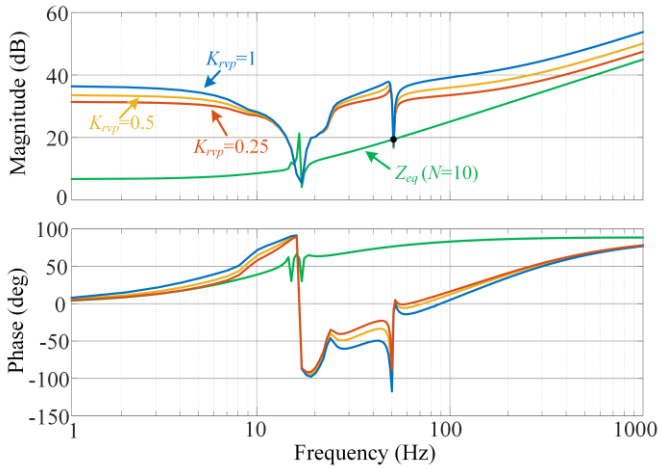

Fig. 15. Impact of the proportional gain of the railway-side voltage controller on the AC/AC MMC impedance.

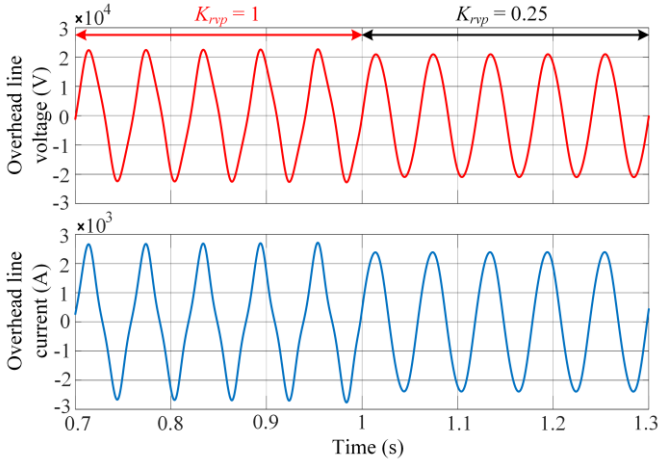

Fig. 16. Simulation results of overhead line voltage and current, under the step change from K_{rvp} = 1 to K_{rvp} = 0.25 at t =1 s.

Fig. 16 shows the simulation results of the railway system under 10 operating trains, where the proportional gain of the railway voltage controller is modified at t = 1s. It can be seen that the system operates with significant oscillations when K_{rvp} = 1. While, when K_{rvp} is decreased from 1 to 0.25 at 1s, the system becomes stable without oscillations.

As the above analysis shows, the value range of the control parameters for ensuring the stability of railway system can be obtained based on the stability analysis. In regards to the optimal design of control parameters, not only the system stability but also the dynamic response should be considered. The tradeoff between the system stability and dynamic response speed can be further studied in the future work.

VI. Conclusions

This paper develops the impedance model of AC/AC MMC for the electric railway system. The proposed impedance model considers the internal harmonics within AC/AC MMC and the control model, and thus this model can accurately reflect the characteristics of AC/AC MMC for railway traction power supply. Meanwhile, the proposed model is compared with the impedance model ignoring the steady-state harmonics. The results show that the steady-state ripples of capacitor voltage in

the modeling is a key factor ensuring the accuracy of the model. In addition, the stability of the MMC-based railway system is analyzed using the proposed impedance model. The impedance of AC/AC MMC shows a capacitive behavior in the low frequency range, and thus the system is prone to oscillate when multiple trains operate simultaneously. To damp the oscillations, the impact of parameters of railway-side voltage controller on AC/AC MMC impedance characteristics is analyzed, and it is found that decreasing proportional gain can increase the phase margin of the AC/AC MMC-based railway system. This result can provide guidance for the controller parameter design of MMC to improve the stability of AC/AC MMC-based railway system.

APPENDIX I: REVIEW OF THE HSS METHOD

For any time-varying periodic signal $x(t)$, it can be written in the form of Fourier series as below

$$x(t)=\sum_{n\in Z} X_n e^{jn\omega_1 t}$$

where X_n is the Fourier coefficient, ω_1 is the fundamental angular frequency of the signal.

The time-domain state-space equation of the system is expressed as

$$\dot{x}(t)=A(t)x(t)+B(t)u(t)$$

Based on Fourier series and harmonic balance theory [30], the time-domain state-space equation of the system can be transformed to the frequency-domain state-space equation, which is expressed as

$$s\boldsymbol{X}=(\boldsymbol{A}-\boldsymbol{N})\boldsymbol{X}+\boldsymbol{B}\boldsymbol{U}$$

where

$$\boldsymbol{X}=\left[X_{-n},\cdots,X_{-1},X_0,X_1,\cdots,X_n\right]^T$$

$$\boldsymbol{U}=\left[U_{-n},\cdots,U_{-1},U_0,U_1,\cdots,U_n\right]^T$$

$$\boldsymbol{A}=\Gamma\left(A(t)\right)=\begin{bmatrix} A_0 & A_{-1} & \cdots & A_{-n} & & & \\ A_1 & \ddots & \ddots & \ddots & \ddots & & \\ \vdots & \ddots & A_0 & A_{-1} & \ddots & \ddots & \\ A_n & \ddots & A_1 & A_0 & A_{-1} & \ddots & A_{-n} \\ & \ddots & \ddots & A_1 & A_0 & \ddots & \vdots \\ & & \ddots & \ddots & \ddots & \ddots & A_{-1} \\ & & & A_n & \cdots & A_1 & A_0 \end{bmatrix}$$

$$\boldsymbol{B}=\Gamma\left(B(t)\right)$$

$$\boldsymbol{N}=diag\left[-jn\omega_1\boldsymbol{I},\cdots,-j\omega_1\boldsymbol{I},\boldsymbol{O},j\omega_1\boldsymbol{I},\cdots,jn\omega_1\boldsymbol{I}\right]$$

$\boldsymbol{I}$ and $\boldsymbol{O}$ are the identity matrix and zero matrix having the same matrix size with the number of state variables. The subscript n indicates the order of the harmonic, X_n, U_n, A_n, B_n are the nth Fourier coefficients of $x(t)$, $u(t)$, $A(t)$ and $B(t)$, respectively. $\boldsymbol{A}$ and $\boldsymbol{B}$ are the Toeplitz matrix to make the frequency-domain convolution operation easier. The Toeplitz matrix is denoted as the function Γ in this paper. The matrix A_n of the Toeplitz matrix $\boldsymbol{A}$ has the same size as $A(t)$.

APPENDIX II: PARAMETERS OF THE ELECTRIC TRAIN SYSTEM

TABLE IV
PARAMETERS OF THE TRAIN-NETWORK SYSTEM

Power supply parameters		
v_s	Secondary side voltage of the onboard transformer	1 p.u. (2 kV)
k	Onboard transformer ratio	7.5
f_1	Network voltage frequency	50/3 Hz
V_{DC}	DC voltage of the 4QC	2 p.u.
L	Input inductor of the 4QC	0.325 p.u
R_d	Load resistance	4 p.u.
C_d	DC-link capacitance	1.1875 p.u.
L_C	Catenary network equivalent inductance	1.3 p.u.
R_C	Catenary network equivalent resistance	0.3125 p.u.
Controller parameters		
$H_{DC}(s)$	DC-link voltage controller	0.05+0.1/s
$H_i(s)$	Current controller	0.1+0.5/s
BW_{PLL}	PLL bandwidth	10 Hz

REFERENCES

[1] D. Ronanki and S. S. Williamson, "Modular Multilevel Converters for Transportation Electrification: Challenges and Opportunities," *IEEE Trans. Transport. Electrifi.*, vol. 4, no. 2, pp. 399-407, June 2018.

[2] D. Ronanki, S. A. Singh and S. S. Williamson, "Comprehensive Topological Overview of Rolling Stock Architectures and Recent Trends in Electric Railway Traction Systems," *IEEE Trans. Transport. Electrifi*, vol. 3, no. 3, pp. 724-738, Sept. 2017.

[3] M. A. Perez, S. Bernet, J. Rodriguez, S. Kouro and R. Lizana, "Circuit Topologies, Modeling, Control Schemes, and Applications of Modular Multilevel Converters," *IEEE Trans. Power Electron.*, vol. 30, no. 1, pp. 4-17, Jan. 2015.

[4] S. Debnath, J. Qin, B. Bahrani, M. Saeedifard and P. Barbosa, "Operation, Control, and Applications of the Modular Multilevel Converter: A Review," *IEEE Trans. Power Electron.*, vol. 30, no. 1, pp. 37-53, Jan. 2015.

[5] A. Steimel, "Power-electronic grid supply of ac railway systems," in *Proc. 13th Int. Conf. Optimiz. Electr. Electron. Equip*., May 2012, pp. 16–25.

[6] M. Winkelnkemper, A. Korn, and P. Steimer, "A modular direct converter for transformerless rail interties," in *Proc. Int. Symp. on Ind. Electron*., Jul. 2010, pp. 562–567.

[7] M. A. Perez, J. Rodriguez, E. J. Fuentes and F. Kammerer, "Predictive Control of AC-AC Modular Multilevel Converters," *IEEE Trans. Ind. Electron.*, vol. 59, no. 7, pp. 2832-2839, July 2012.

[8] M. Lei *et al*., "Full Degree of Freedom Based Control Scheme of the Single-Phase Direct AC-AC Modular Multilevel Converter for Railway Power Conditioning Under Asymmetric Branch Conditions," *IEEE Trans. Ind. Electron.*, vol. 67, no. 3, pp. 1671-1683, March 2020.

[9] F. Ma *et al*., "A Railway Traction Power Conditioner Using Modular Multilevel Converter and Its Control Strategy for High-Speed Railway System," *IEEE Trans. Transport. Electrifi*., vol. 2, no. 1, pp. 96-109, March 2016.

[10] W. Liu, K. Zhang, X. Chen and J. Xiong, "Simplified model and submodule capacitor voltage balancing of single-phase AC/AC modular multilevel converter for railway traction purpose," *IET Power Electron.*, vol. 9, no. 5, pp. 951-959, 20 4 2016.

[11] S. SONG, J. LIU, S. OUYANG, X. CHEN and B. LIU, "Control of Direct AC/AC Modular Multilevel Converter in Railway Power Supply System," *IPEC-Niigata 2018 -ECCE Asia*, 2018, pp. 1051-1055.

[12] J. Sun, "Impedance-Based Stability Criterion for Grid-Connected Inverters," *IEEE Trans. Power Electron*, vol. 26, no. 11, pp. 3075-3078, Nov. 2011.

[13] B. Wen, D. Dong, D. Boroyevich, R. Burgos, P. Mattavelli, and Z. Shen, "Impedance-based analysis of grid-synchronization stability for three-phase paralleled converters," *IEEE Trans. Power Electron*., vol. 31, no. 1, pp. 26-38, Jan. 2016.

[14] J. Sun and H. Liu, "Sequence impedance modeling of modular multilevel converters," *IEEE J. Emerg. Sel. Top. Power Electron*., vol. 5, no. 4, pp. 1427–1443, Dec. 2017.

[15] J. Lyu, X. Zhang, X. Cai and M. Molinas, "Harmonic State-Space Based Small-Signal Impedance Modeling of a Modular Multilevel Converter With Consideration of Internal Harmonic Dynamics," *IEEE Trans. Power Electron.*, vol. 34, no. 3, pp. 2134-2148, March 2019.

[16] L. Bessegato, K. Ilves, L. Harnefors and S. Norrga, "Effects of Control on the AC-Side Admittance of a Modular Multilevel Converter," *IEEE Trans. Power Electron.*, vol. 34, no. 8, pp. 7206-7220, Aug. 2019.
[17] Z. Li *et al*., "Accurate Impedance Modeling and Control Strategy for Improving the Stability of DC System in Multiterminal MMC-Based DC Grid," *IEEE Trans. Power Electron.*, vol. 35, no. 10, pp. 10026-10049, Oct. 2020.
[18] Z. Xu *et al*., "A Complete HSS-Based Impedance Model of MMC Considering Grid Impedance Coupling," *IEEE Trans. Power Electron.*, vol. 35, no. 12, pp. 12929-12948, Dec. 2020.
[19] L. Bessegato, K. Ilves, L. Harnefors, S. Norrga and S. Östlund, "Control and Admittance Modeling of an AC/AC Modular Multilevel Converter for Railway Supplies," *IEEE Trans. Power Electron.*, vol. 35, no. 3, pp. 2411-2423, March 2020.
[20] J. Luo, X. Zhang, Y. Xue, K. Gu and F. Wu, "Harmonic Analysis of Modular Multilevel Matrix Converter for Fractional Frequency Transmission System," *IEEE Trans. Power Del*., vol. 35, no. 3, pp. 1209-1219, June 2020.
[21] L. Harnefors, A. Antonopoulos, S. Norrga, L. Ängquist, and H.P. Nee, "Dynamic analysis of modular multilevel converters," *IEEE Trans. Ind. Electron*., vol. 60, no. 7, pp. 2526-2537, Jul. 2013.
[22] K. Ilves, A. Antonopoulos, S. Norrga, and H.P. Nee, "Steady-state analysis of interaction between harmonic components of arm and line quantities of modular multilevel converters," *IEEE Trans. Power Electron*., vol. 27, no. 1, pp. 57-68, Jan. 2012.
[23] J. R. C. Orillaza and A. R. Wood, "Harmonic state-space model of a controlled TCR," *IEEE Trans. Power Del*., vol. 28, no. 1, pp. 197-205, Jan. 2013.
[24] J. Kwon, X. Wang, F. Blaabjerg, C. L. Bak, V. S. Sularea, and C. Busca, "Harmonic interaction analysis in a grid-connected converter using harmonic state-space (HSS) modeling," *IEEE Trans. Power Electron*., vol. 32, no. 9, pp. 6823-6835, Sept. 2017.
[25] L. Angquist, A. Antonopoulos, D. Siemaszko, K. Ilves, M. Vasiladiotis and H. Nee, "Open-Loop Control of Modular Multilevel Converters Using Estimation of Stored Energy," *IEEE Trans. Ind. Appl.*, vol. 47, no. 6, pp. 2516-2524, Nov.-Dec. 2011.
[26] S. Danielsen, O. B. Fosso, M. Molinas, et al, "Simplified models of a single-phase power electronic inverter for railway power system stability analysis—development and evaluation," *Electric Power Systems Research*, vol. 80, no. 2, pp. 204-214, Feb. 2010.
[27] H. Hu, H. Tao, F. Blaabjerg, X. Wang, Z. He, and S. Gao, "Train–network interactions and stability evaluation in high-speed railways—Part I: Phenomena and modeling," *IEEE Trans. Power Electron*., vol. 33, no. 6, pp. 4627–4642, Jun. 2018.
[28] H. Zhang, Z. Liu, S. Wu and Z. Li, "Input Impedance Modeling and Verification of Single-Phase Voltage Source Converters Based on Harmonic Linearization," *IEEE Trans. Power Electron.*, vol. 34, no. 9, pp. 8544-8554, Sept. 2019.
[29] C. Zhang, M. Molinas, S. Føyen, J. A. Suul and T. Isobe, "Harmonic-Domain SISO Equivalent Impedance Modeling and Stability Analysis of a Single-Phase Grid-Connected VSC," *IEEE Trans. Power Electron.*, vol. 35, no. 9, pp. 9770-9783, Sept. 2020.
[30] N. M. Wereley, "Analysis and control of linear periodically time varying systems," Ph.D. dissertation, Dept. of Aeronautics and Astronautics, MIT, 1991.

Yixing Wang was born in Henan, China, 1993. He received the B.S. degree in Electrical Engineering and Automation in Electrical Engineering from Hunan University, Changsha, in 2016. Since 2018, he has been working toward the Ph.D. degree at the College of Electrical and Information Engineering, Hunan University, Changsha, China.
His main research interests include modular multilevel converter, impedance modeling, stability analysis.

Qianming Xu (M'17) was born in Henan, China, in 1989. He received the B.S. degree in electrical engineering and automation and the Ph.D. degree in electrical engineering from Hunan University, Changsha, China, in 2012 and 2017, respectively.
Since 2019, he has been an Associate Professor with the College of Electrical and Information Engineering, Hunan University, Changsha, China.
His research interests include multilevel converter, power electronic reliability monitoring, and power quality control.

Shuhan Liao (S'18-M'20) was born in Xiangtan, Hunan Province, China, in 1993. She received B. Eng. Degree and the Ph. D Degree in electrical engineering from Wuhan University, Wuhan, China, in 2015 and 2020, respectively. From Oct. 2018 to Oct. 2019, she was a guest Ph. D. student with the Department of Energy Technology, Aalborg University, Aalborg, Denmark.
She is currently a Postdoctoral Researcher at Hunan University, Changsha, China. Her main research interests include the modeling and dynamic analysis of renewable energy generation systems.

Lei Wang (M'17-SM'20) received the B.Sc. degree in Electrical and Electronics Engineering from University of Macau (UM), Macao SAR, P. R. China, in 2011, M.Sc. degree in Electronics Engineering from Hong Kong University of Science and Technology (HKUST), Hong Kong SAR, P. R. China, in 2012. and Ph.D. degree in Electrical and Computer Engineering from University of Macau (UM), Macao SAR, P. R. China, in 2017.
He was a postdoctoral fellow in the Power Electronics Laboratory of UM from Jan. 2017 to Feb. 2019. He was a visiting fellow in department of electrical and computer engineering, University of Auckland, from Feb. 2019 to Aug. 2019. In 2019, he joined College of Electrical and Information Engineering, Hunan University, Changsha, China, where he is currently a Full Professor.
He has authored 1 Springer books, 1 Elsevier book chapter, 5 patents (U.S.A and China) and over 40 journal and conference papers. Dr. Wang received the champion award in the "Schneider Electric Energy Efficiency Cup", Hong Kong, 2011, Macao Science and Technology R&D Award for Postgraduates (Ph.D) in 2018.

Josep M. Guerrero (S'01-M'04-SM'08-FM'15) received the B.S. degree in telecommunications engineering, the M.S. degree in electronics engineering, and the Ph.D. degree in power electronics from the Technical University of Catalonia, Barcelona, in 1997, 2000 and 2003, respectively. Since 2011, he has been a Full Professor with the Department of Energy Technology, Aalborg University, Denmark. From 2015 he is a distinguished guest Professor in Hunan University.
His research interests mainly include power electronics, distributed energy-storage, and microgrids. Prof. Guerrero is an Associate Editor for the IEEE TRANSACTIONS ON POWER ELECTRONICS, the IEEE TRANSACTIONS ON INDUSTRIAL ELECTRONICS, and the IEEE Industrial Electronics Magazine, and an Editor for the IEEE TRANSACTIONS on SMART GRID and IEEE TRANSACTIONS on ENERGY CONVERSION.
In 2014, 2015, and 2016 he was awarded by Thomson Reuters as Highly Cited Researcher, and in 2015 he was elevated as IEEE Fellow for his contributions on distributed power systems and microgrids.